Granular Matter 4, 17–24 © Springer-Verlag 2002
DOI 10.1007/s10035-001-0097-8

Monte Carlo simulation of the homogeneous cooling state for a granular mixture

José María Montanero, Vicente Garzó

Abstract The Direct Simulation Monte Carlo (DSMC) method is used to numerically solve the Enskog equation for a granular binary mixture in the homogeneous cooling state (HCS). The fourth velocity moments, the temperature ratio, and also the velocity distribution functions are obtained and compared with approximate analytical results derived recently from a Sonine polynomial expansion [V. Garzó and J. W. Dufty, Phys. Rev. E **60**, 5706 (1999)]. The comparison shows an excellent agreement between both approaches, even for strong dissipation or disparate values of the mechanical parameters of the mixture. In contrast to previous studies, the partial temperatures of each species are clearly different, so that the total energy is not equally distributed between both species. Finally, in the same way as in the one-component case, the simulation as well as the theory show a high energy tail of the distribution functions.

Keywords Kinetic and transport theory of gases, Monte Carlo simulation, Granular mixtures

1 Introduction

A simple and realistic way of capturing the effects of dissipation in rapid granular flows is through a system of smooth hard spheres with inelastic collisions [1]. The binary collisions are specified in terms of the change in relative velocity at contact, but with a decrease in the magnitude of the normal component measured through a positive restitution coefficient. In the context of kinetic theory, the Boltzmann and Enskog equations have been conveniently modified to account for inelastic binary collisions. These equations have been used to derive the corresponding fluid dynamic equations with explicit expressions for the transport coefficients [2,3]. The standard procedure to get them is the Chapman-Enskog expansion [4] adapted to the case of inelastic collisions. For a given kinetic equation, the use of the Chapman-Enskog method leads to a *normal* solution in which all the space and time dependence occurs through the hydrodynamic fields.

In the case of elastic collisions, the Chapman-Enskog solution is obtained as an expansion around the local Maxwellian, while for inelastic collisions the reference state is a local *cooling* solution with a monotonically time decreasing temperature. For spatially homogeneous states, the latter is referred to as the homogeneous cooling state (HCS). Since the HCS qualifies as a normal solution, all its time dependence is only through the temperature. Nevertheless, in spite of the simplicity of the HCS, no exact solution of the Boltzmann or Enskog equations describing such a state is known. For a one-component system, an approximate form for the distribution function based in a Sonine polynomial expansion has been obtained [5], showing an excellent agreement with Monte Carlo simulations of the Enskog equation [6,7]. In general, the results indicate that the deviations from Gaussian behavior in the HCS are quite small so that, the Maxwell distribution can be considered as a good approximation for the region of thermal velocities. In the large velocity region, some analytical studies [5,8] have found that the decay of the distribution function is not Gaussian but exponential. This high energy tail has been also confirmed by simulations in the case of hard disks [9].

In the context of granular binary mixtures, the studies are more scarce. Needless to say, the analysis of properties of fluid mixtures is considerably more complicated than in the case of a one-component system. Not only the number of mechanical parameters of the system is larger but, in addition, the inelasticity of collisions among all pairs must be characterized by three independent coefficients of normal restitution. To the best of our knowledge, the only theoretical study of the HCS for a granular mixture has been recently made by Garzó and Dufty [10]. In a similar way as the one-component fluid [5], the set of coupled Enskog equations admits a scaling solution in which the time dependence of the distribution functions occurs entirely through the temperature of the mixture. An important and surprising result is that the partial temperatures of each species (measuring their mean kinetic energies) are *different*, although their cooling rates are equal. This effect is generic for multicomponent systems and is a consequence of the inelasticity and the mechanical

Received: 9 May 2001

José María Montanero (✉)
Departamento de Electrónica e Ingeniería Electromecánica,
Universidad de Extremadura,
E-06071 Badajoz, Spain

Vicente Garzó
Departamento de Física,
Universidad de Extremadura,
E-06071 Badajoz, Spain

V. Garzó acknowledges partial support from the DGES (Spain) through Grant No. BFM2001-0718.

differences of the particles (e.g., masses, diameters). This result contrasts with previous studies in granular mixtures [11–14], where the equality of the partial temperatures was assumed. The velocity distribution functions for each species are approximately determined by using again a Sonine polynomial expansion around Maxwellians, which are defined in terms of the temperature for that species. Our results are restricted to the first Sonine approximation, and show that the non-Maxwellian corrections have small effects on the cooling rates and on the temperature ratio at all inelasticities. However, the corresponding reference Maxwellians for the two species are quite different due to temperature differences.

Since all the above conclusions have been obtained from an approximate solution, an interesting problem is to numerically solve the Enskog equation in the HCS in order to test the reliability of such an analytical solution. In this present paper, we use the Direct Monte Carlo Simulation (DSMC) method [15] to solve the Enskog equation in the HCS. Although this method was originally devised for elastic fluids, its extension to deal with granular gases is very easy. From the simulations it is possible to compute the velocity distribution functions over a quite wide range of velocities. In particular, precise values of the fourth-velocity moments and of the temperature ratio are obtained. The evaluation of this latter quantity is one of the main objectives of this paper. In addition, and as a complementary result, we are also interested in computing the high energy tails for the distributions and compare them with the theoretical predictions.

The paper is organized as follows. The theoretical analysis is reviewed in Sec. 2. The computer simulation method employed to numerically solve the (uniform) Enskog equation is described in Sec. 3. In Sec. 4, the results are presented and compared with the theoretical predictions. The comparison shows a quite good agreement indicating that the first Sonine approximation provides an accurate description over a quite wide range of values of the mechanical parameters of the mixture as well as of the restitution coefficients. Finally, we close the paper in Sec. 5 with some concluding remarks.

2
Theoretical predictions

We consider a binary mixture of smooth inelastic hard spheres of masses m_1 and m_2 and diameters σ_1 and σ_2. In the special case of spatially homogeneous isotropic states, the velocity distribution functions $f_i(\mathbf{v}_1;t)$ $(i=1,2)$ obey the set of nonlinear Enskog kinetic equations:

$$\frac{\partial}{\partial t}f_i(v_1,t)=\sum_j J_{ij}\left[v_1|f_i(t),f_j(t)\right] \ , \tag{1}$$

where the Enskog collision operator $J_{ij}\left[v_1|f_i,f_j\right]$ describing the scattering of pairs of particles is

$$J_{ij}\left[v_1|f_i,f_j\right]=\chi_{ij}\sigma_{ij}^2\int d\mathbf{v}_2\int d\widehat{\boldsymbol{\sigma}}\,\Theta(\widehat{\boldsymbol{\sigma}}\cdot\mathbf{g}_{12})(\widehat{\boldsymbol{\sigma}}\cdot\mathbf{g}_{12}) \times\left[\alpha_{ij}^{-2}f_i(v_1',t)f_j(v_2',t) -f_i(v_1,t)f_j(v_2,t)\right] \ . \tag{2}$$

Here, χ_{ij} is the pair correlation function for particles of type i and j when they are in contact, i.e., separated by $\sigma_{ij}=(\sigma_i+\sigma_j)/2$. Also, $\widehat{\boldsymbol{\sigma}}$ is a unit vector along their line of centers, Θ is the Heaviside step function, $\mathbf{g}_{12}=\mathbf{v}_1-\mathbf{v}_2$, and $\alpha_{ij}\leq 1$ is the coefficient of normal restitution for collisions between particles of species i and j. In addition, the primes on the velocities denote the initial values $\{\mathbf{v}_1',\mathbf{v}_2'\}$ that lead to $\{\mathbf{v}_1,\mathbf{v}_2\}$ following a binary collision:

$$\mathbf{v}_1'=\mathbf{v}_1-\mu_{ji}\left(1+\alpha_{ij}^{-1}\right)(\widehat{\boldsymbol{\sigma}}\cdot\mathbf{g}_{12})\widehat{\boldsymbol{\sigma}} \ , \tag{3}$$

$$\mathbf{v}_2'=\mathbf{v}_2+\mu_{ij}\left(1+\alpha_{ij}^{-1}\right)(\widehat{\boldsymbol{\sigma}}\cdot\mathbf{g}_{12})\widehat{\boldsymbol{\sigma}} \ , \tag{4}$$

where $\mu_{ij}=m_i/\left(m_i+m_j\right)$. Note that for the spatially homogeneous case, the only difference between the Enskog equation (1) for dense systems and the Boltzmann equation for dilute systems is the presence of the factor χ_{ij}, which accounts for the increase of the collision frequency for collisions between species i and j due to excluded volume effects.

The collision operators conserve particle number of each species and the total momentum, but the total energy is not conserved. This implies that

$$\sum_{i,j}\int d\mathbf{v}_1\frac{1}{2}m_iv_1^2J_{ij}[v_1|f_i,f_j]=-\frac{3}{2}nT\zeta \ , \tag{5}$$

where ζ is identified as the "cooling rate" due to inelastic collisions among all species. Here, $n=n_1+n_2$,

$$n_i=\int d\mathbf{v}_1 f_i(v_1) \tag{6}$$

is the number density of species i, and

$$T=\sum_i x_iT_i=\frac{1}{n}\sum_i\int d\mathbf{v}_1\frac{m_i}{3}v_1^2f_i(v_1) \ , \tag{7}$$

is the temperature of the mixture. In addition, $x_i=n_i/n$ is the molar fraction of species i, and Eq. (7) also defines the partial temperature T_i of species i. This quantity measures the mean kinetic energy of species i. At a kinetic level, it is also convenient to discuss energy transfer in terms of the "cooling rates" ζ_i for the partial temperatures T_i. They are defined as

$$\zeta_i=-\frac{2}{3n_iT_i}\sum_j\int d\mathbf{v}_1\frac{1}{2}m_iv_1^2J_{ij}[v_1|f_i,f_j] \ . \tag{8}$$

From the Enskog equation (1) and Eq. (8), it is easy to get the identities:

$$\zeta_i=-\frac{\partial}{\partial t}\ln T_i, \quad \zeta=-\frac{\partial}{\partial t}\ln T \ . \tag{9}$$

The time evolution of the temperature ratio $\gamma=T_1(t)/T_2(t)$ follows from the the first equality of Eq. (9):

$$\frac{\partial}{\partial t}\ln\gamma=\zeta_2-\zeta_1 \ . \tag{10}$$

Furthermore, according to Eqs. (7) and (9), the total cooling rate ζ can be expressed in terms of the coolings ζ_i as

$$\zeta=T^{-1}\sum_i x_iT_i\zeta_i \ . \tag{11}$$

Regardless of the initial uniform state, the solution to the Enskog equation (1) tends to the so-called homogeneous cooling state (HCS), characterized by the fact that all the time dependence of $f_i(v_1;t)$ occurs only through the temperature $T(t)$. Consequently, $f_i(v_1;t)$ has the form

$$f_i(v_1;t) = n_i v_0^{-3}(t)\Phi_i\left(v_1/v_0(t)\right) \ , \tag{12}$$

where $v_0(t) = \sqrt{2T(t)(m_1+m_2)/(m_1m_2)}$ is a thermal velocity defined in terms of the temperature of the mixture $T(t)$. The fact that f_i depends on time only through $T(t)$ (*normal* solution) necessarily implies that the temperature ratio γ must be a constant (independent of time) in the HCS. According to Eq. (10), this means that the cooling rates must be equal, i.e., $\zeta_1(t) = \zeta_2(t)$. In the elastic case, where f_i is a Maxwellian, the above condition leads to $T_1(t) = T_2(t) = T(t)$, and so the granular energy is equally distributed between both species (equipartition of energy). However, in the case of inelastic collisions, the equality of the cooling rates leads in general to different partial temperatures, even if one considers the Maxwellian approximation to f_i. This does not mean that there are additional hydrodynamic degrees of freedom since the partial kinetic temperatures still can be expressed in terms of the total temperature T as

$$T_1(t) = \frac{\gamma}{1+x_1(\gamma-1)}T(t) \ , \tag{13}$$

$$T_2(t) = \frac{1}{1+x_1(\gamma-1)}T(t) \ . \tag{14}$$

In the HCS, the dimensionless Enskog equations with Eq. (12) read

$$\frac{1}{2}\zeta_i^*\frac{\partial}{\partial \mathbf{v}_1^*}\cdot(\mathbf{v}_1^*\Phi_i) = \sum_j J_{ij}^*[v_1^*|\Phi_i,\Phi_j] \ , \tag{15}$$

where $v_{1,2}^* = v_{1,2}/v_0$, $\zeta_i^* = \zeta_i/(n\sigma_{12}^2 v_0)$ and

$$\begin{aligned} J_{ij}^*[v_1^*|\Phi_i,\Phi_j] &\equiv \frac{v_0^2}{nn_i\sigma_{12}^2}J_{ij}[v_1|f_i,f_j] \\ &= x_j\chi_{ij}\left(\frac{\sigma_{ij}}{\sigma_{12}}\right)^2\int d\mathbf{v}_2^*\int d\widehat{\boldsymbol{\sigma}}\,\Theta(\widehat{\boldsymbol{\sigma}}\cdot\mathbf{g}_{12}^*) \\ &\quad\times(\widehat{\boldsymbol{\sigma}}\cdot\mathbf{g}_{12}^*)[\alpha_{ij}^{-2}\Phi_i(v_1'^*)\Phi_j(v_2'^*) \\ &\quad-\Phi_i(v_1)\Phi_j(v_2)] \ . \end{aligned} \tag{16}$$

In the same way as in the one-component case [5], there is no exact solution to Eqs. (15). Accurate approximate forms for the distributions Φ_i may be obtained using low order truncation of expansions in a series of Sonine polynomials. The leading order in the Sonine expansion is [10]

$$\begin{aligned} \Phi_i(v_1^*) \to &\left(\frac{\lambda_i}{\pi}\right)^{3/2}e^{-\lambda_i v_1^{*2}} \\ &\left[1+\frac{c_i}{4}\left(\lambda_i^2 v_1^{*4}-5\lambda_i v_1^{*2}+\frac{15}{4}\right)\right]. \end{aligned} \tag{17}$$

Here, $\lambda_i = T/(T_i\mu_{ji})$ and the coefficients c_i must be determined from the Enskog equations. These coefficients (which are directly related to the fourth velocity moments of f_i) measure the deviation of the distribution Φ_i from the chosen reference Maxwellian.

In order to get the coefficients c_i, first one substitutes Eq. (17) into the Enskog equations (15), multiplies that equation by v_1^{*4}, and then integrates over the velocity. Since the values of c_i are expected to be very small, only linear terms in c_i are retained. Therefore, one gets a coupled set of linear equations, which can be easily solved. Next, these coefficients are substituted into the condition of equality of cooling rates ($\zeta_1 = \zeta_2$) to obtain a nonlinear function determining the temperature ratio γ. This provides entirely all the parameters of the distributions Φ_i and the temperatures T_i in terms of the restitution coefficients and the mechanical parameters of the mixture [10]. The expressions of the above quantities are quoted in Appendix A.

Based on the comparison performed in the one-component case between theory [5] and simulation [7,9], one expects that the distribution function is well described by the simplest Sonine approximation (17), at least in the region of thermal velocities (say, $v_1^* \sim 1$). This point will be confirmed in Sec. 4 when we compare our theory with Monte Carlo simulations. Nevertheless, for velocities higher than the thermal one, the above approach is not accurate. For a single granular gas, van Noije and Ernst [5] and Esipov and Pöschel [8] have found a high energy tail of the velocity distribution function in the HCS. The corresponding derivation in the case of a binary mixture proceeds along similar lines. If a particle of species i is a fast particle ($v_1^* \gg 1$), the dominant contributions to the collision integral J_{ij}^* are collisions in which particles of species j have velocities typically in the thermal range, so that the relative velocity $\mathbf{g}_{12}^*$ in the collision integral J_{ij}^* can be replaced by $\mathbf{v}_1^*$. Further, by the same arguments as in Ref. [5], the gain term of J_{ij}^* can be neglected versus the loss term. The collision integral J_{ij}^* then reduces to

$$J_{ij}^*[v_1^*|\Phi_i,\Phi_j] \approx -\pi x_j\chi_{ij}\left(\frac{\sigma_{ij}}{\sigma_{12}}\right)^2 v_1^*\Phi_i(v_1^*) \ . \tag{18}$$

In this case, the Enskog equations (15) simplifies to

$$\frac{1}{2}\zeta_i^*\left(3+\mathbf{v}_1^*\cdot\frac{\partial}{\partial\mathbf{v}_1^*}\right)\Phi_i(v_1^*) = -\beta_i v_1^*\Phi_i(v_1^*) \ , \tag{19}$$

where β_i is given by

$$\beta_i = \pi\sum_j x_j\chi_{ij}\left(\frac{\sigma_{ij}}{\sigma_{12}}\right)^2 \ . \tag{20}$$

For large v_1^*, the first term on the left hand side of Eq. (19) can be neglected with respect to the right hand side, and the solution of Eq. (19) has the form

$$\Phi_i(v_1^*) \sim \mathscr{A}_i\exp\left(-\frac{2\beta_i}{\zeta_i^*}v_1^*\right) \ , \tag{21}$$

where $\mathscr{A}_i$ is an undetermined integration constant. In the case of mechanically equivalent particles, Eq. (21) reduces to the results derived in Refs. [5] and [8]. Clearly, Eq. (21) shows an *overpopulation* with respect to the Maxwell-Boltzmann tail.

3
Direct Simulation Monte Carlo method

The Direct Simulation Monte Carlo (DSMC) method devised by Bird [15] has proven to be the most convenient algorithm to solve numerically the Boltzmann equation. Recently, Montanero and Santos [16] have extended the DSMC method to solve the Enskog equation for a system of elastic hard spheres. The application of this algorithm to a mixture of inelastic hard spheres is straightforward.

In the case of the freely evolving state, the procedure can be summarized as follows. The velocity distribution function of the species i is represented by the velocities $\{\mathbf{v}_k\}$ of N_i "simulated" particles:

$$f_i(\mathbf{v},t) \to n_i \frac{1}{N_i} \sum_{k=1}^{N_i} \delta(\mathbf{v}-\mathbf{v}_k(t)) \ . \tag{22}$$

Note that the number of particles N_i must be chosen according to the relation $N_i/N_j = n_i/n_j$. At the initial state, one assigns velocities to the particles drawn from a certain probability distribution. Since the system is assumed to be spatially homogeneous, the velocities of the particles change only due to binary collisions. Consequently, only the collision stage needs to be considered in the DSMC algorithm. The collisions are simulated over a time step Δt which is much smaller than the mean free time. Binary interactions between particles of species i and j must be considered. To simulate the collisions between particles of species i with j a sample of $\frac{1}{2}N_i\omega_{\max}^{(ij)}\Delta t$ pairs is chosen at random with equiprobability. Here, $\omega_{\max}^{(ij)}$ is an upper bound estimate of the probability that a particle of the species i collides with a particle of the species j. Let us consider a pair $\{k,\ell\}$ belonging to this sample. Here, k denotes a particle of species i and ℓ a particle of species j. For each pair $\{k,\ell\}$ with velocities $\{\mathbf{v}_k,\mathbf{v}_\ell\}$, the following steps are taken: (1) a given direction $\widehat{\boldsymbol{\sigma}}_{k\ell}$ is chosen at random with equiprobability; (2) the collision between particles k and ℓ is accepted with a probability equal to $\Theta(\mathbf{g}_{k\ell}\cdot\widehat{\boldsymbol{\sigma}}_{k\ell})\omega_{k\ell}^{(ij)}/\omega_{\max}^{(ij)}$, where $\omega_{k\ell}^{(ij)} = 4\pi\sigma_{ij}^2 n_j \chi_{ij}|\mathbf{g}_{k\ell}\cdot\widehat{\boldsymbol{\sigma}}_{k\ell}|$ and $\mathbf{g}_{k\ell} = \mathbf{v}_k - \mathbf{v}_\ell$; (3) if the collision is accepted, postcollisional velocities are assigned to both particles according to the scattering rules:

$$\mathbf{v}_k \to \mathbf{v}_k - \mu_{ji}(1+\alpha_{ij})(\mathbf{g}_{k\ell}\cdot\widehat{\boldsymbol{\sigma}}_{k\ell})\widehat{\boldsymbol{\sigma}}_{k\ell} \ , \tag{23}$$

$$\mathbf{v}_\ell \to \mathbf{v}_\ell + \mu_{ij}(1+\alpha_{ij})(\mathbf{g}_{k\ell}\cdot\widehat{\boldsymbol{\sigma}}_{k\ell})\widehat{\boldsymbol{\sigma}}_{k\ell} \ . \tag{24}$$

In the case that in one of the collisions $\omega_{k\ell}^{(ij)} > \omega_{\max}^{(ij)}$, the estimate of $\omega_{\max}^{(ij)}$ is updated as $\omega_{\max}^{(ij)} = \omega_{k\ell}^{(ij)}$. The procedure described above is performed for $i = 1,2$ and $j = 1,2$.

It must be stressed again that we have solved the *homogeneous* set of Enskog equations, as given in Eq. (19). Because of positions of the particles do not appear in Eq. (19), we have considered a single cell and so there is no need to compute and store them. As a consequence, the possible formation of spatial inhomogeneities (particle clusters) is eliminated in our simulations. This capacity of the DSMC method for forcing the mixture to stay in the HCS (even for strong dissipation) allows us to identify and measure for instance, the high velocity tails.

The physical quantities are evaluated by averaging over the particles and also over an ensemble of $\mathscr{N}$ independent realizations or replicas. The initial state was that specified by the Maxwell-Boltzmann probability distribution:

$$f_i(\mathbf{v},0) = n_i \ \pi^{-3/2} \ v_{0i}^{-3}(0)\exp\left(-v^2/v_{0i}^2(0)\right) \ , \tag{25}$$

where $v_{0i}^2(0) = 2T_i(0)/m_i$ is the thermal velocity of species i and $T_i(0)$ is the corresponding initial temperature. Also, the Carnahan-Starling approximation for χ_{ij} has been used [17]:

$$\chi_{ij} = \frac{1}{1-\nu} + \frac{3}{2}\frac{\xi}{(1-\nu)^2}\frac{\sigma_{ii}\sigma_{jj}}{\sigma_{ij}} + \frac{1}{2}\frac{\xi^2}{(1-\nu)^3}\left(\frac{\sigma_{ii}\sigma_{jj}}{\sigma_{ij}}\right)^2 \ , \tag{26}$$

where $\xi = (\pi n/6)\sum_i x_i\sigma_{ii}^2$, and $\nu = (\pi n/6)\sum_i x_i\sigma_{ii}^3$ is the volume packing fraction.

In our simulations we have typically taken a total number of particles $N = N_1 + N_2 = 10^5$ and a number of replicas $\mathscr{N} = 10$. Since the thermal velocity decreases monotonically with time, we have taken a time-dependent time step $\Delta t = 3 \times 10^{-3}\lambda_{11}/v_{01}(t)$, where $\lambda_{11} = (\sqrt{2}\pi n_1\chi_{11}\sigma_{11}^2)^{-1}$ is the mean free path for collisions 1–1.

A full presentation of the results is difficult since there are many parameters involved in the problem: α_{ij}, $\mu \equiv m_1/m_2$, $\delta \equiv n_1/n_2$, $w \equiv \sigma_{11}/\sigma_{22}$, and $n^* \equiv n\sigma_{12}^3$. For the sake of simplicity, henceforth we will consider the case $\alpha_{11} = \alpha_{22} = \alpha_{12} \equiv \alpha$. After an initial transient period, one expects that the distribution functions $\Phi_i(v_1^*)$ reach stationary values independent of the initial conditions. This hydrodynamic regime must be identified as the HCS. Although we are mainly focused on evaluating all the physical relevant quantities of the problem in the steady state, it is also interesting to analyze the time evolution of some of these quantities. Perhaps, the most interesting is the temperature ratio γ, which measures the lack of equipartition of energy between both species. To illustrate the approach to the HCS, in Fig. 1 we present the time evolution of the temperature ratio $\gamma(t) = T_1(t)/T_2(t)$ for $n^* = 0$, $\delta = 2$, $w = 1$, and $\mu = 10$. We have considered two different cases: $\alpha = 0.5$ (a) (inelastic fluid), and $\alpha = 1$ (b) (elastic fluid). After a transient regime, we observe that both curves converge to different steady values. While in the elastic case both temperatures tend to be the same ($\gamma = 1$), no "equilibration" occurs for inelastic collisions since the partial temperatures are clearly different ($\gamma \simeq 3.8$). In addition, the corresponding steady values practically coincide with those predicted by the Sonine solution described in Sec. 3. The same qualitative behavior has been found for the scaling property (12) of the distribution function. Therefore, in the following we will focus on the dependence of the steady values of the reduced quantities on the restitution coefficient α and the parameters of the mixture.

4
Results

By using the numerical method described in the previous section, we have computed the steady state values of the

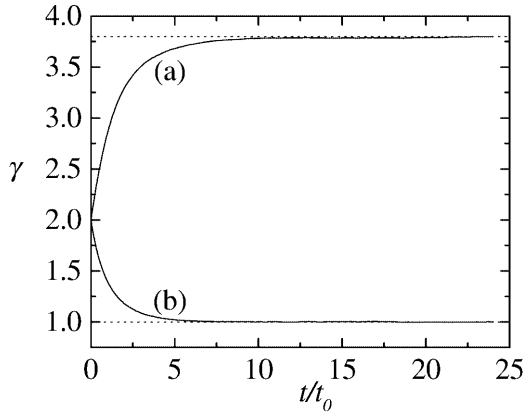

Fig. 1. Time evolution of $\gamma(t) = T_1(t)/T_2(t)$ for $n^* = 0$, $\delta = 2$, $w = 1$, $\mu = 10$, and $\alpha = 0.5$ (a) and $\alpha = 1$ (b). The dotted lines refer to the theoretical predictions. Time is measured in units of $t_0 \equiv \lambda_{11}/v_{01}(0)$

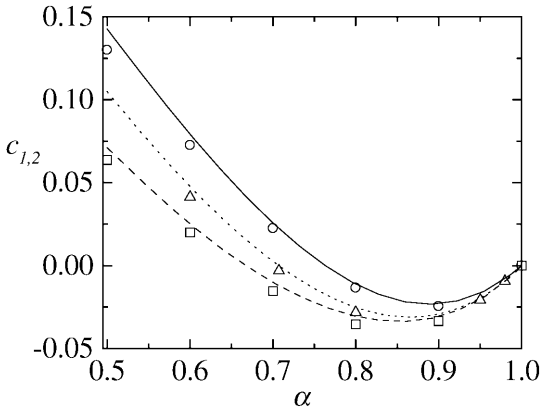

Fig. 2. Plot of the coefficients c_i versus the restitution coefficient α for $n^* = 0$, $\delta = 1$, $w = 1$ and $\mu = 2$. The solid line and the circles refer to c_1 while the dashed line and the squares correspond to c_2. The dotted line and the triangles refer to the common value in the single component case. The lines are the theoretical predictions and the symbols correspond to the simulation results

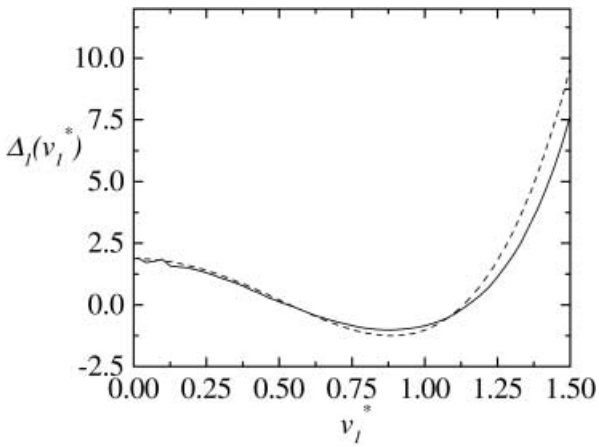

Fig. 3. Plot of the simulation values of the function $\Delta_1(v_1^*)$ defined by Eq. (27) for $\alpha = 0.5$, $n^* = 0$, $\delta = 1/2$, $w = 1$ and $\mu = 4$. The dashed line is the Sonine polynomial (28)

coefficients c_i, the temperature ratio γ, and the distribution functions $\Phi_i(v_1^*)$ for several values of the restitution coefficient α, the mass ratio $\mu \equiv m_1/m_2$, the concentration ratio $\delta \equiv n_1/n_2$, the ratio of sizes $w \equiv \sigma_{11}/\sigma_{22}$, and the reduced density n^*. These results will be compared with those obtained from the first Sonine approximation described in Sec. 2 and Appendix A.

The basic quantity measuring the deviation of the distribution functions from the corresponding Maxwellians are the cumulants c_i. In Fig. 2, we show the dependence of c_1 and c_2 on α for $n^* = 0$, $\delta = 1$, $w = 1$, and $\mu = 2$. The simulation data has been obtained in homogeneous conditions. We also present the corresponding result for the one-component system (mechanically equivalent particles, i.e., $w = 1$ and $\mu = 1$). The agreement between the simulation data and the theoretical predictions are excellent. The small values of these coefficients support the assumption of a low-order truncation in polynomial expansion and indicates that the distribution functions $\Phi_i(v_1/v_0(t))$ for thermal velocities are well represented by the Sonine approximation (17). To confirm this, we have measured the deviation of Φ_i from the corresponding Maxwellian. More precisely, we have evaluated the function $\Delta_i(v_1^*)$ defined by the relation

$$\Phi_i(v_1^*) = \left(\frac{\lambda_i}{\pi}\right)^{3/2} e^{-\lambda_i v_1^{*2}} \left[1 + \frac{1}{2} c_i \Delta_i(v_1^*)\right] \quad . \tag{27}$$

The function $\Delta_1(v_1^*)$ is plotted in Fig. 3 for $\alpha = 0.5$, $n^* = 0$, $\delta = 1/2$, $w = 1$, and $\mu = 4$. The dashed line is the first Sonine approximation

$$\Delta_1(v_1^*) \to \tfrac{1}{2}\lambda_i^2 v_1^{*4} - \tfrac{5}{2}\lambda_i v_1^{*2} + \tfrac{15}{8} \quad . \tag{28}$$

As could be expected, the simulation curve agrees very well with the corresponding Sonine polynomial, confirming the accuracy of the solution (17) in the region of thermal velocities.

One of the main new results of this description is that the partial temperatures are different ($\gamma \neq 1$). This conclusion contrasts with all the previous results derived for granular mixtures [11–14], where it was implicitly assumed the equipartition of granular energy between both species (i.e., $\gamma = 1$). In Figs. 4, 5, and 6 we plot the temperature ratio γ versus the restitution coefficient α for different choices of the mechanical parameters characterizing the mixture. The theory as well as the simulation results clearly indicate that γ is different from unity, even for weak inelasticity. Figure 4 shows the dependence of γ on α for $n^* = 0$, $\delta = 2$, $w = 1$, and for several values of the mass ratio. The agreement between theory and simulation is very good, implying the accuracy of the expression of γ obtained in the first Sonine approximation. For large differences in the mass ratio, the temperature differences are significant. As can be observed in Fig. 5, the influence of the concentration ratio δ on the temperature ratio γ is not as strong as in that observed with the mass ratio, although is still quite important. The dependence of the relative temperature ratio $\gamma(\alpha, n^*)/\gamma(\alpha, 0)$ on the density n^* is plotted in Fig. 6 for $\delta = 1/2$, $w = 2$, $\mu = 2$ and two different vales of α: $\alpha = 0.6$ and 0.8. We see that, for a given value of the density, the relative temperature ratio decreases as the degree of inelasticity increases. It is

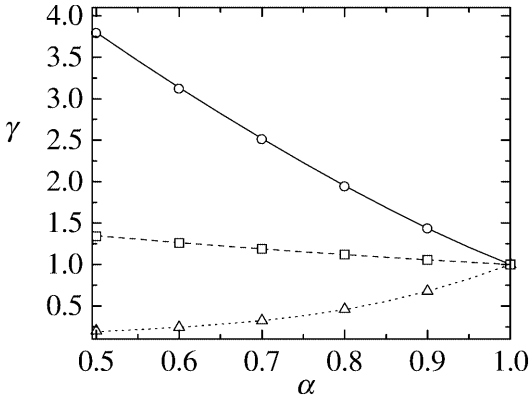

Fig. 4. Plot of the temperature ratio γ versus the restitution coefficient α for $n^* = 0$, $\delta = 2$, $w = 1$ and three different values of the mass ratio: $\mu = 1/10$ (dotted line and triangles), $\mu = 2$ (dashed line and squares) and $\mu = 10$ (solid line and circles). The lines are the theoretical predictions and the symbols correspond to the simulation results

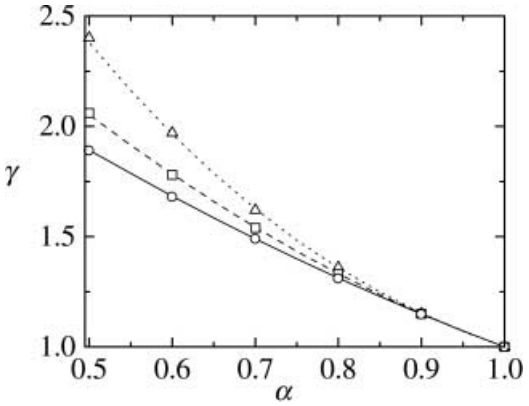

Fig. 5. Plot of the temperature ratio versus the restitution coefficient α for $n^* = 0$, $w = 1$, $\mu = 4$ and three different values of the concentration ratio: $\delta = 1/4$ (dotted line and triangles), $\delta = 1$ (dashed line and squares) and $\delta = 4$ (solid line and circles). The lines are the theoretical predictions and the symbols correspond to the simulation results

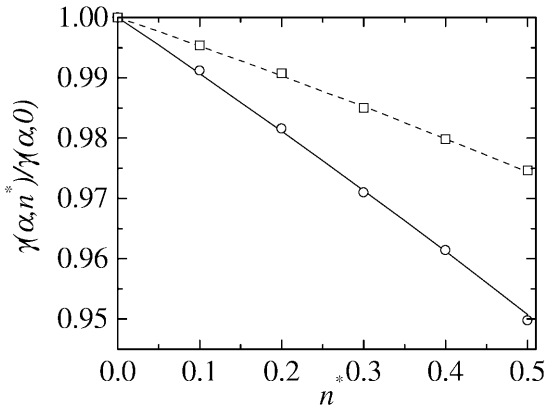

Fig. 6. Plot of the relative temperature ratio $\gamma(\alpha, n^*)/\gamma(\alpha, 0)$ as a function of the reduced density n^* for $\delta = 1/2$, $w = 2$, $\mu = 2$ and two different values of the restitution coefficient: $\alpha = 0.6$ (solid line and circles) and $\alpha = 0.8$ (dashed line and squares). The lines are the theoretical predictions and the symbols correspond to the simulation results

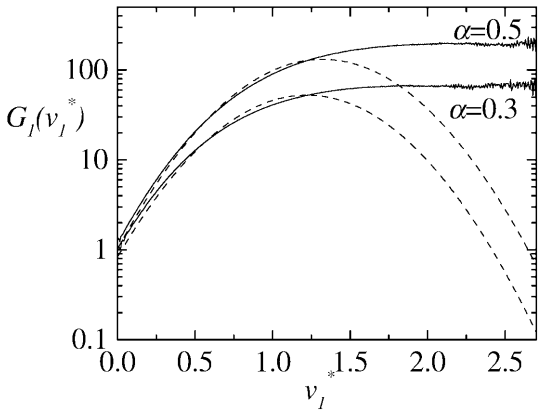

Fig. 7. Plot of the simulation values of the function $G_1(v_1^*)$ defined by Eq. (30) for $\alpha = 0.3$ and 0.5, $n^* = 0$, $\delta = 1/2$, $w = 1$ and $\mu = 4$. The dashed line are the Maxwell-Boltzmann predictions

evident again the excellent agreement between the Sonine predictions and the simulation data.

As a final point, it is interesting to analyze the possible high energy tail of the distributions Φ_i from the simulation results. This could confirm the theoretical predictions given by Eq. (21). Needless to say, this result is much harder to confirm in the simulations since it involves a very small fraction of particles. Equation (21) implies that

$$\lim_{v_1^* \to \infty} G_i(v_1^*) = \mathscr{A}_i = \text{const} \ , \tag{29}$$

where

$$G_i(v_1^*) \equiv \exp\left(\frac{2\beta_i v_1^*}{\zeta_i^*}\right) \Phi_i(v_1^*) \ . \tag{30}$$

The function $G_1(v_1^*)$ is plotted (in logarithmic scale) in Fig. 7 for $\alpha = 0.3$ and 0.5, $n^* = 0$, $\delta = 1/2$, $w = 1$ and $\mu = 4$. The agreement with the prediction (29) is excellent in both cases. The region of large velocities is overpopulated with respect to the Maxwell-Boltzmann distribution. Thus, for instance, at $v_1^* = 2.2$, $\Phi/\Phi_{\text{MB}} \simeq 37$ for $\alpha = 0.5$, Φ_{MB} being the corresponding Maxwell-Boltzmann distribution.

5 Concluding remarks

In this paper we have performed Monte Carlo simulations of the Enskog equation for a granular binary mixture in the homogeneous cooling state (HCS). One of the primary objectives of this work has been to check the accuracy of a recent analytical solution obtained by Garzó and Dufty [10] by using a first Sonine approximation. To put this work in a proper context, it must be noticed that we have simulated directly the spatially uniform equation (1) so that the appearance of the so-called cluster instability [18] is precluded in our simulations.

The simulation results have confirmed the velocity scaling and form assumed for the distribution functions in the HCS [c.f. Eq. (12)]. A consequence of this scaling form is that all temperatures are proportional to each

other with the same cooling rate. This does not mean that the temperatures themselves are the same, and indeed the theory and the simulation data show they are different. In general, the simulation results are in very good agreement with the Sonine solution, showing the reliability and accuracy of the analytical predictions even for strong dissipation or disparate values of the ratios of mass, concentration, and sizes.

The fact that the fourth velocity moments c_i, defined through Eq. (17), are small and qualitatively similar to that of the one-component case [5], suggests that the distribution functions for each species are close to a Maxwellian *at the temperature for that species*. Nevertheless, both Maxwellians are very different due to the temperature differences. The simulation results indicate that the temperature ratio γ presents a complex dependence on the parameters of the problem. This complexity is well captured by the Sonine approximation, as it is shown in Figs. 4, 5, and 6. As said before, this conclusion differs from previous results derived in granular mixtures for which $\gamma = 1$. According to the results obtained here, the deviations from the energy equipartition ($T_1/T_2 \neq 1$) can be weak or strong depending on the mechanical differences between the species and the degree of inelasticity in collisions. In addition, the simulations have also confirmed the overpopulation predicted for large velocities by means of a simple theoretical analysis.

Finally, let us mention that the study made here can stimulate the performance of Monte Carlo simulations of granular mixtures in order to provide information about the stability of the HCS. This is important since it is known that the HCS for a one-component system is unsta ble to long-wavelength perturbations. These simulations must be complemented by theoretical analyses based on hydrodynamics equations obtained via the Chapman-Enskog method for states close to the HCS [19]. This allows us to know whether the mixture is more or less stable and whether new active mechanisms (e.g. segregation) appear in the system. Work along these lines are in progress.

A
Some explicit expressions in the first Sonine approximation

In this Appendix, we will quote the expressions of the coefficients c_1 and c_2 and the temperature ratio γ obtained by using the first Sonine polynomial approximation (17). Henceforth, it will be understood that dimensionless quantities will be used and the asterisks will be deleted to simplify the notation. The coefficients c_1 and c_2 can be written as

$$c_1 = \frac{AG - ED}{BG - DF} \ , \tag{31}$$

$$c_2 = \frac{BE - AF}{BG - DF} \ , \tag{32}$$

where

$$A = -\frac{15}{2\lambda_1^2}\zeta_1^{(0)} - \Lambda_1^{(0)} \ , \tag{33}$$

$$B = \frac{15}{2\lambda_1^2}\left(\zeta_{11}^{(1)} + \frac{1}{2}\zeta_1^{(0)}\right) + \Lambda_{11}^{(1)} \ , \tag{34}$$

$$D = \frac{15}{2\lambda_1^2}\zeta_{12}^{(1)} + \Lambda_{12}^{(1)} \ , \tag{35}$$

$$E = -\frac{15}{2\lambda_2^2}\zeta_2^{(0)} - \Lambda_2^{(0)} \ , \tag{36}$$

$$F = \frac{15}{2\lambda_2^2}\zeta_{21}^{(1)} + \Lambda_{21}^{(1)} \ , \tag{37}$$

$$G = \frac{15}{2\lambda_2^2}\left(\zeta_{22}^{(1)} + \frac{1}{2}\zeta_2^{(0)}\right) + \Lambda_{22}^{(1)} \ . \tag{38}$$

In the above equations, we have introduced the quantities [10]

$$\zeta_1^{(0)} = \frac{2}{3}\sqrt{2\pi}\left(\frac{\sigma_{11}}{\sigma_{12}}\right)^2 x_1\chi_{11}\lambda_1^{-1/2}(1-\alpha_{11}^2) + \frac{4}{3}\sqrt{\pi}x_2\chi_{12}\mu_{21}\left(\frac{1+\eta}{\eta}\right)^{1/2}(1+\alpha_{12})\lambda_2^{-1/2} \times [2-\mu_{21}(1+\alpha_{12})(1+\eta)] \ , \tag{39}$$

$$\zeta_{11}^{(1)} = \frac{1}{8}\frac{\sqrt{\pi}}{2}\left(\frac{\sigma_{11}}{\sigma_{12}}\right)^2 x_1\chi_{11}\lambda_1^{-1/2}(1-\alpha_{11}^2) + \frac{1}{12}\sqrt{\pi}x_2\chi_{12}\mu_{21}\frac{(1+\eta)^{-3/2}}{\eta^{1/2}}(1+\alpha_{12})\lambda_2^{-1/2} \times [2(3+4\eta)-3\mu_{21}(1+\alpha_{12})(1+\eta)] \ , \tag{40}$$

$$\zeta_{12}^{(1)} = -\frac{1}{12}\sqrt{\pi}x_2\chi_{12}\mu_{21}\left(\frac{1+\eta}{\eta}\right)^{-3/2}(1+\alpha_{12})\lambda_2^{-1/2} \times [2+3\mu_{21}(1+\alpha_{12})(1+\eta)] \ , \tag{41}$$

$$\Lambda_1^{(0)} = -\sqrt{2\pi}\lambda_1^{-5/2}\Big\{x_1\chi_{11}\left(\frac{\sigma_{11}}{\sigma_{12}}\right)^2\frac{9+2\alpha_{11}^2}{2}\left(1-\alpha_{11}^2\right) - \sqrt{2}x_2\chi_{12}\left(1+\eta\right)^{-1/2}\mu_{21}\left(1+\alpha_{12}\right)\big[-2\left(6+5\eta\right) + \mu_{21}\left(1+\alpha_{12}\right)\left(1+\eta\right)\left(14+5\eta\right) - 8\mu_{21}^2\left(1+\alpha_{12}\right)^2 \times\left(1+\eta\right)^2 + 2\mu_{21}^3\left(1+\alpha_{12}\right)^3\left(1+\eta\right)^3\big]\Big\} \ , \tag{42}$$

$$\Lambda_{11}^{(1)} = -\sqrt{2\pi}\lambda_1^{-5/2}\Big\{x_1\chi_{11}\left(\frac{\sigma_{11}}{\sigma_{12}}\right)^2\Big[1+\alpha_{11} + \frac{3}{64}\left(69+10\alpha_{11}^2\right)\left(1-\alpha_{11}^2\right)\Big] - \frac{\sqrt{2}}{16}x_2\chi_{12} \times\left(1+\eta\right)^{-5/2}\mu_{21}\left(1+\alpha_{12}\right)\big[-2(90+231\eta+184\eta^2 + 40\eta^3) + 3\mu_{21}\left(1+\alpha_{12}\right)\left(1+\eta\right)\left(70+117\eta + 44\eta^2\right) - 24\mu_{21}^2\left(1+\alpha_{12}\right)^2\left(1+\eta\right)^2\left(5+4\eta\right) + 30\mu_{21}^3\left(1+\alpha_{12}\right)^3\left(1+\eta\right)^3\big]\Big\} \ , \tag{43}$$

$$\Lambda_{12}^{(1)} = \frac{\sqrt{\pi}}{8}x_2\chi_{12}\lambda_1^{-5/2}\eta^2\left(1+\eta\right)^{-5/2}\mu_{21}\left(1+\alpha_{12}\right) \times\big[2\left(2+5\eta\right)+3\mu_{21}\left(1+\alpha_{12}\right)\left(1+\eta\right)\left(2+5\eta\right) - 24\mu_{21}^2\left(1+\alpha_{12}\right)^2\left(1+\eta\right)^2 + 30\mu_{21}^3\left(1+\alpha_{12}\right)^3 \times\left(1+\eta\right)^3\big] \ . \tag{44}$$

In these equations, $\eta = \lambda_1/\lambda_2 = \mu_{12}/(\mu_{21}\gamma)$. The corresponding expressions for $\zeta_2^{(0)}$, $\zeta_{22}^{(1)}$, $\zeta_{21}^{(1)}$, $\mathbf{\Lambda}_2^{(0)}$, $\mathbf{\Lambda}_{22}^{(1)}$, and $\mathbf{\Lambda}_{21}^{(1)}$ can be easily obtained from Eqs. (39)–(44), respectively, by interchanging 1 and 2 and setting $\eta \to \eta^{-1}$.

Once the coefficients c_i are given in terms of γ and the parameters of the mixture, the temperature ratio γ can be explicitly obtained by numerically solving the condition for equal cooling rates:

$$\zeta_1^{(0)} + \zeta_{11}^{(1)} c_1 + \zeta_{12}^{(1)} c_2 = \zeta_2^{(0)} + \zeta_{22}^{(1)} c_2 + \zeta_{21}^{(1)} c_1 \ . \tag{45}$$

References

1. C. S. Campbell, Ann. Rev. Fluid Mech. 22 (1990), p. 57
2. J. J. Brey, J. W. Dufty, C. S. Kim & A. Santos, Phys. Rev. E 58 (1998), p. 4638
3. V. Garzó & J. W. Dufty, Phys. Rev. E 59 (1999), p. 5895
4. J. Ferziger & H. Kaper, *Mathematical Theory of Transport Processes in Gases* (North-Holland, Amsterdam, 1972)
5. T. P. C. van Noije & M. H. Ernst, Gran. Matt. 1 (1998), p. 57
6. J. J. Brey, M. J. Ruiz-Montero & D. Cubero, Phys. Rev. E 54 (1996), p. 3664
7. J. M. Montanero & A. Santos, Gran. Matt. 2 (2000), p. 53
8. S. E. Esipov & T. Pöschel, J. Stat. Phys. 86 (1997), p. 1385
9. J. J. Brey, D. Cubero & M. J. Ruiz-Montero, Phys. Rev. E 59 (1999), p. 1256
10. V. Garzó & J. W. Dufty, Phys. Rev. E 60 (1999), p. 5706
11. J. T. Jenkins & F. Mancini, Phys. Fluids A 1 (1989), p. 2050
12. P. Zamankhan, Phys. Rev. E 52 (1995), p. 4877
13. B. Arnarson & J. T. Willits, Phys. Fluids 10 (1998), p. 1324
14. J. T. Willits & B. Arnarson, Phys. Fluids 11 (1999), p. 3116
15. G. Bird, *Molecular Gas Dynamics and the Direct Simulation of Gas Flows* (Clarendon, Oxford, 1994)
16. J. M. Montanero & A. Santos, Phys. Rev. E 54 (1996), p. 438; Phys. Fluids 9 (1997), p. 2057
17. E. W. Grundke & D. Henderson, Mol. Phys. 24 (1972), p. 269; L. L. Lee and D. Levesque, Mol. Phys. 26 (1973), p. 1351
18. S. M. McNamara & W. R. Young, Phys. Fluids A 5 (1993), p. 34; Phys. Rev. E 50 (1994), p. R28; I. Goldhirsch & G. Zanetti, Phys. Rev. Lett. 70 (1993), p. 1619; N. Sela & I. Goldhirsch, Phys. Fluids 7 (1995), p. 507
19. V. Garzó & J. W. Dufty, cond-mat 0105395